Highly Transparent and Flexible Organic Light-Emitting Diodes with Structure Optimized for Anode/Cathode Multilayer Electrodes

*Dong-Young Kim, Yun Cheol Han, Hyun Cheol Kim, Eun Gyo Jeong, and Kyung Cheol Choi**

In this study, a dielectric layer/metal/dielectric layer (multilayer) electrode is proposed as both anode and cathode for use in the fabrication of transparent and flexible organic light-emitting diodes (TFOLEDs). The structure of multilayer electrodes is optimized by systematic experiments and optical calculations considering the transmittance and efficiency of the device. The details of the multilayer electrode structure are [ZnS (24 nm)/Ag (7 nm)/MoO_3 (5 nm)] and [ZnS (3 nm)/Cs_2CO_3 (1 nm)/Ag (8 nm)/ZnS (22 nm)], as anode and cathode, respectively. The optimized TFOLED design is fabricated on a polyethylene terephthalate (PET) substrate, and the device shows high transmittance (74.22% around 550 nm) although the PET substrate has lower transmittance than glass. The TFOLEDs operate normally under compressive stress; degradation of electrical characteristics is not observed, comparable to conventional OLEDs with ITO and Al as electrodes. In addition, because the fabricated TFOLEDs show a nearly Lambertian emission pattern and a negligible shift of Commission International de l'Eclairage (CIE) coordination, it is concluded that the fabricated TFOLEDs are suitable for use in displays.

1. Introduction

In recent years, the transparent and flexible display is in the best interest of researchers as future display.[1] Organic light-emitting diodes (OLEDs), in particular, are considered promising candidates for advanced displays due to their capability to satisfy both transparent and flexible properties.[2] However, OLEDs typically consist of brittle indium tin oxide (ITO)[3] and metal film of low transparency, so alternative electrodes are required to produce transparent, flexible OLEDs (TFOLEDs).[4] Several kinds of conductive electrodes, including those of transparent conductive oxide,[5] metal nanowires,[6] metal grids,[7] graphene,[8] carbon nanotubes,[9] and conducting polymer,[10] have been investigated for their possible use as alternative electrodes. However, their lack of flexibility, low transmittance, and high sheet resistance, has made it difficult to apply these alternative electrodes to TFOLEDs.

On the other hand, there is a kind of electrode that consists of a high refractive index dielectric layer/metal film/high refractive index dielectric layer (multilayer). It exhibits high transmittance, high flexibility, and low sheet resistance. In particular, the high refractive index dielectric layers of the multilayer improve transmittance by reducing reflection of the metal film caused by destructive interference.[11] Previous studies on multilayer electrodes started from work on heat reflective optical filters.[12] So far, several research groups have reported various structures of multilayer electrodes (ZnS/Ag/ZnS,[13] WO_3/Ag/MoO_3,[14] ZnS/Ag/MoO_3,[15] Cs_2CO_3/Ag/ZnS[16] applied to OLEDs. However, these studies utilized the Ag films with thickness greater than 10 nm. The thickness of this Ag film might hinder fabrication of highly transparent OLEDs, because increase in the thickness of the Ag film is used to compensate for reduction of transmittance in devices.[13,17] Therefore, the determination of an optimally minimum thickness for continuous, low sheet resistance Ag films is crucial for fabrication of highly transparent devices.[18] Also, in previous studies, the multilayer electrodes were applied as either anodes or cathodes because the devices could not have transparency and flexibility at the same time. If applied to both sides, the thickened metal films cause reduced transmittance and caused angular dependency by the microcavity effect.[19,20] Therefore, it is first necessary to solve the problems found in previous studies in order to fabricate effective TFOLEDs.

In this paper, we propose a TFOLED structure using multilayer electrodes as both anode and cathode at the same time. In order to overcome the limitations of previous multilayer electrodes, the highly transparent device was fabricated using thin, continuous, Ag film between dielectric layers. Furthermore, by using an electron-only device and optical simulation, the structure of the TFOLEDs was optimized without degradation of efficiency. We also demonstrated that the fabricated TFOLEDs had little influence on angular dependency by investigating the electroluminescence (EL) intensity spectra and Commission International de l'Eclairage (CIE) coordination, at varying emission angles.

D.-Y. Kim, Y. C. Han, H. C. Kim, E. G. Jeong, Prof. K. C. Choi
Department of Electrical Engineering
KAIST
291 Daehak-ro, Yuseong-gu
Daejeon 305-701, South Korea
E-mail: kyungcc@kaist.ac.kr

DOI: 10.1002/adfm.201502542

2. Results and Discussion

2.1. Fabrication of Highly Transparent Multilayer Anode

It is well known that dielectric layers or particles under the thin Ag film, function as a seed layer to reduce the minimum film thickness required to obtain continuous Ag film.[21] However, the relationships between dielectric layers and Ag film thickness are not clearly known. Thus, in this study, the relationship between dielectric layers and Ag film thickness was investigated and the structure of the anode determined.

Figure 1 shows scanning electron microscopy (SEM) images of the surface morphology of Ag film on different types of dielectric (ZnS, MoO_3, WO_3) layers, and on bare glass.[22] The sheet resistance and surface coverage of the Ag films on the dielectric layers were improved compared to Ag films on bare glass. This results from the difference in the surface energy of the dielectric layers. The relatively high surface energy of a dielectric layer can effectively prohibit diffusion from adjacent Ag film and produce a favorable wetting effect for the smoother Ag films.[23] Table S1 of the Supporting Information shows the calculated surface energies of dielectric layers. The surface energy of the ZnS layer (75.94 dyn cm^{-1}) was higher than the others, and the tendency of surface energies of dielectrics correspond well to the tendency of surface morphologies of Ag film (Figure 1). The Ag film on the ZnS layer shows the lowest sheet resistance and highest surface coverage percentage, assuming the same Ag film thickness. From this result, we selected ZnS layer as the best dielectric layer for thin-Ag-film fabrication, and chose a thickness of 7 nm for the Ag film. The ZnS/Ag (7 nm) structure showed sheet resistance of 9.74 Ω sq^{-1}, which is similar to that of the ITO electrodes (near 10 Ω sq^{-1}) generally used for OLED electrodes. In addition, this structure made possible fabrication of a multilayer anode with the highest transmittance found in this work.

In the structure of the multilayer anode, the other dielectric layer on the Ag film is MoO_3 (5 nm thick) embedded on the Ag film. The thin MoO_3 layer can improve low hole injection efficiency caused by the difference from the work function of the Ag film (4.6 eV) and the highest occupied molecular orbital (HOMO) level of *N,N′*-bis (naphthalen-1-yl)-*N,N′*-bis (phenyl)-benzidine (NPB, 5.4 eV),[24] which was used as a hole transporting layer (HTL) in this work. Therefore, the combination of ZnS (*x* nm), Ag (7 nm), and MoO_3 (5 nm) was selected to fabricate highly transparent OLEDs using the new multilayer anode structure.

2.2. Fabrication of Highly Transparent Multilayer Cathode

In order to apply the multilayer structure to the cathode, an additional electron injection layer (EIL) is needed to lower the injection barrier because the electron injection barrier at the Ag/emitting layer (EML) interface is large. Moreover, the

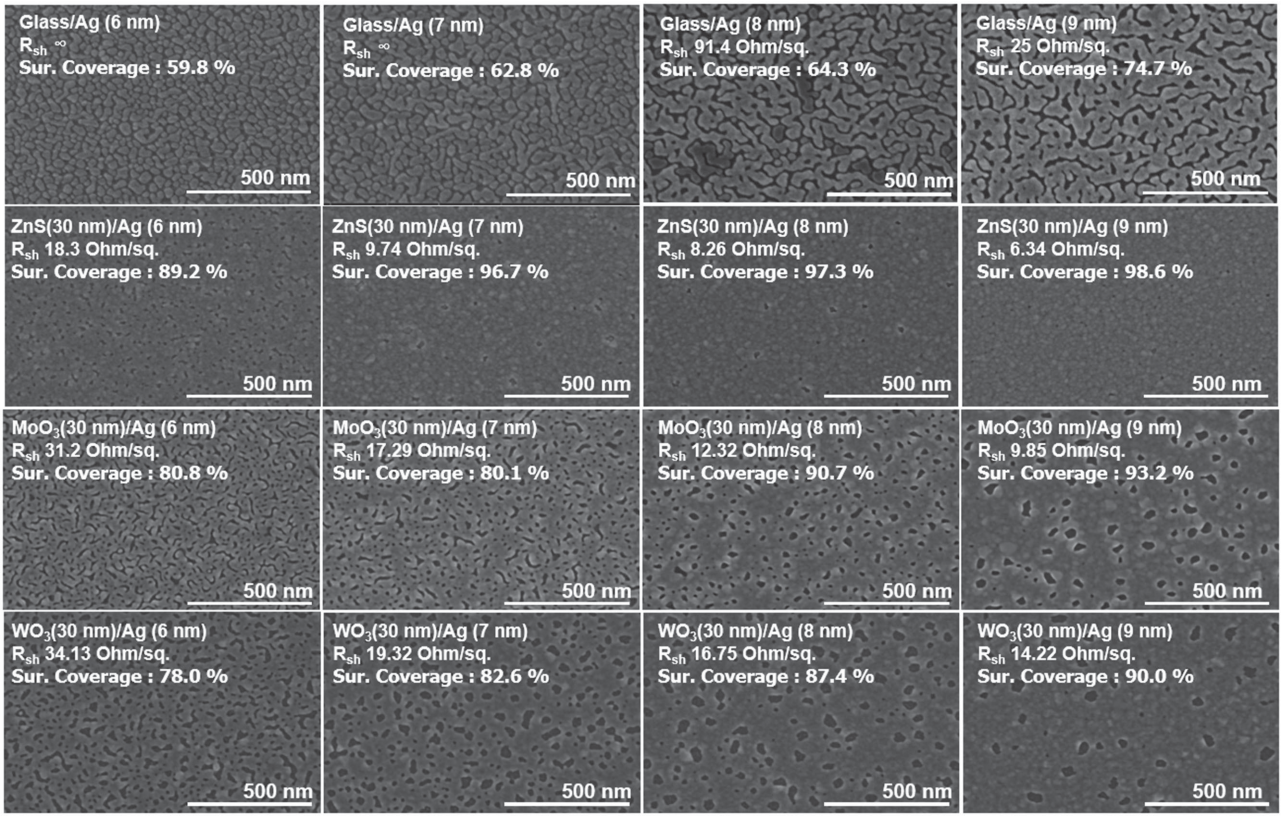

Figure 1. SEM images of the Ag surface: A variety of thicknesses (6, 7, 8, 9 nm) of Ag film deposited on different types of dielectric layers (glass, ZnS, MoO_3, WO_3) with a deposition rate of 2 Å s^{-1}.

additional layer is also required to function as an aid for thin Ag film used in a highly transparent electrode.

In this study, the Cs_2CO_3 and ZnS were deployed between a tris(8-hydroxy-quinolinato) aluminum (Alq_3) layer used as EML, and Ag film used to improve the electron injection efficiency and thin Ag film fabrication. The thin Cs_2CO_3 layer (the EIL) is used to create n-type doping effect on the Alq_3 film and to form the surface dipole at the electrode.[25] As mentioned before, ZnS contributes to better thin Ag film fabrication as well as multilayer anode. However, the conduction band of ZnS and of the lowest unoccupied molecular orbital (LUMO) level of Alq_3 (ZnS: 3.0 eV, Alq_3: 3.0 eV)[26] are similar; therefore, the ZnS thickness must be adjusted to prevent a decrease in the electron injection efficiency. For these reasons, the electron-only devices were fabricated to optimize the electron injection capabilities and transmittance, by varying the thickness of the dielectric layers.

Al was used as anode in all the electron-only devices to prohibit hole injection from anode. The LiF/Al cathode and Ag were used to compare with the multilayer cathode. To measure how the Cs_2CO_3 functions as EIL, a layer of Cs_2CO_3 with three different thicknesses (0.5, 1, and 1.5 nm) was tested. In **Figure 2**a, the Cs_2CO_3 thickness at 1 nm showed the most improved electron injection capability and was higher than that of the LiF/Al and Ag cathode. However, in previous reports, efficient OLEDs were fabricated using LiF/Al as cathodes when the OLEDs structure consisted of NPB and Alq_3 as HTL and EML, respectively.[27,28] For this reason, by adopting the dielectric layer ZnS, we could control electron injection similar to that from LiF/Al, and reduce the minimum film thickness required to obtain continuous Ag film.

In Figure 2b, the electron-only devices were fabricated by splitting the thickness of the ZnS layer (1, 2, 3, 4, and 10 nm).

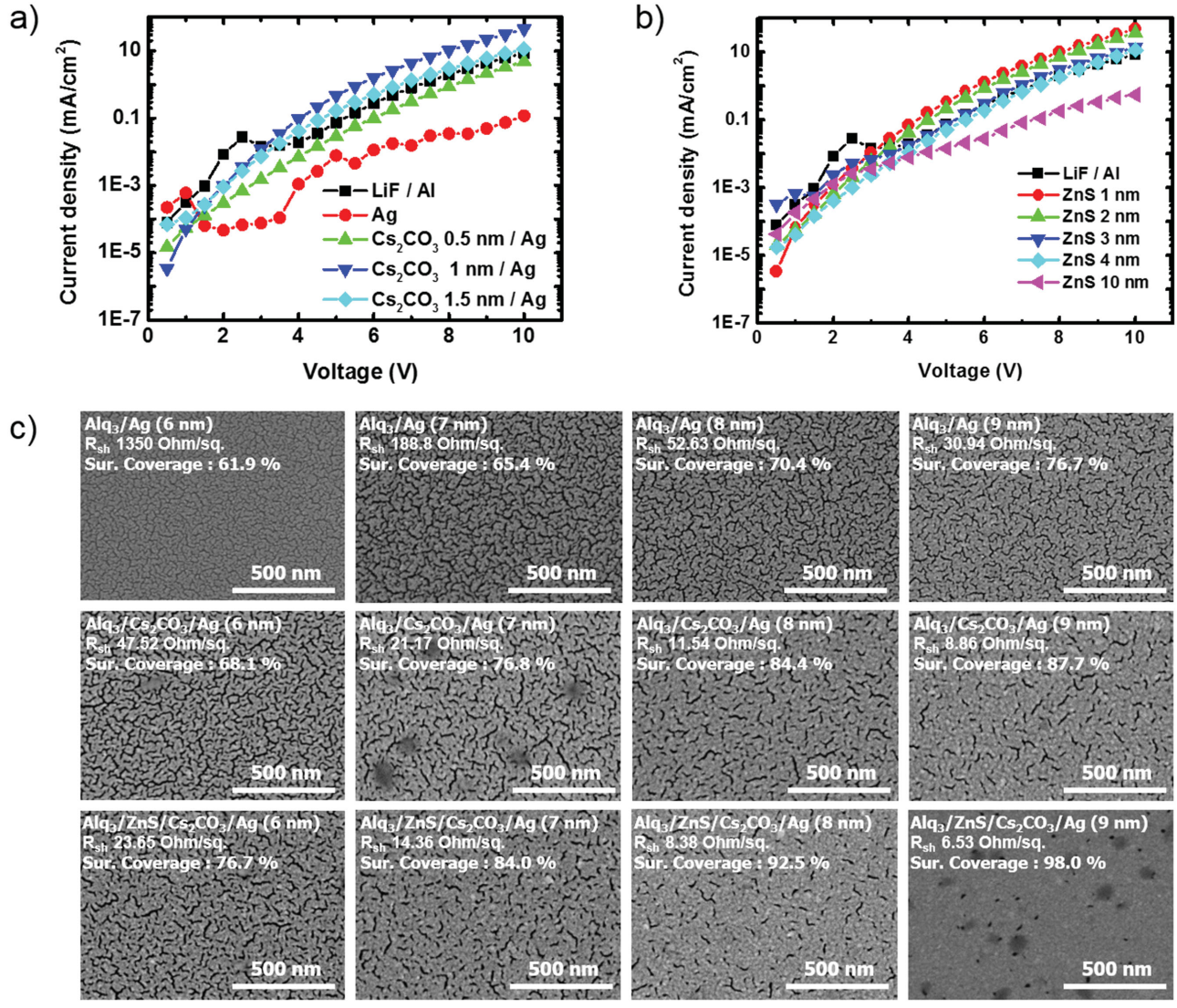

Figure 2. a,b) The current density–voltage (*J*–*V*) characteristics of electron-only devices, a) Al/Alq_3/Cs_2CO_3/Ag with different Cs_2CO_3 thicknesses (0.5, 1, or 1.5 nm) were compared to Al/Alq_3/LiF/Al and Al/Alq_3/Ag, b) Al/Alq_3/ZnS/Cs_2CO_3/Ag with split ZnS thicknesses (1, 2, 3, 4, 10 nm) compared to Al/Alq_3/LiF/Al, c) SEM images of the Ag surface: Ag films with various thicknesses (6, 7, 8, 9 nm) were deposited on dielectric layers (with or without ZnS and Cs_2CO_3).

This showed that increasing the thickness of the ZnS layer reduced the efficiency of electron injection. When ZnS were thicker than 3 nm, the current efficiency of the new devices were lower than that of LiF/Al and the efficiency of OLEDs fabricated from them would also be expected to be low. The electron-only device with a 1 nm Cs_2CO_3 on 3 nm ZnS layer showed similar current efficiency to a LiF/Al device, so we concluded that the multilayer cathode structure: ZnS (3 nm)/Cs_2CO_3 (1 nm)/Ag (x nm)/capping layer, is suitable for OLEDs of high transparency and efficiency.

In order to figure out the effect of dielectric layers on its morphology, Ag films of variable thickness (6, 7, 8, and 9 nm) were deposited on three different types of structure (Figure 2c). Figure 2c shows the surface of Ag films in SEM images. The Ag film with only Cs_2CO_3, showed improved surface morphology compared to those without dielectric layers. This may be because Cs_2CO_3 functions as a nucleation-promoting layer that allows reduction of the minimum film thickness needed to obtain a continuous Ag film, as reported in previous studies.[16] However, the Ag film deposited on the Alq_3 (30 nm)/ZnS (3 nm)/Cs_2CO_3 (1 nm) multilayer showed improved surface morphology along with the lowest sheet resistance and the highest surface coverage percentage, at the same thickness. When the thickness of Ag was 8 nm (sheet resistance 8.38 ohm/sq, surface coverage 92.5%), the multilayer electrode was comparable to the ITO version used in conventional OLEDs. From this, we determined that the structure of the multilayer cathode should be ZnS (3 nm)/Cs_2CO_3 (1 nm)/Ag (8 nm)/capping layer, to achieve high transparency and efficient electron injection. The capping layer deposited on the multilayer cathode layer to improve transmittance will be discussed later.

2.3. Electronic Property of ZnS Layers in Multilayer Electrodes

In order to investigate how a ZnS layer affects the electronic property when the ZnS layer is assembled into the cathode, Alq_3 (50 nm), Alq_3 (50 nm)/ZnS (3 nm), Alq_3 (50 nm)/ZnS (3 nm)/Cs_2CO_3 (1 nm), and Alq_3 (50 nm)/Cs_2CO_3 (1 nm) films were fabricated and X-ray photoelectron spectroscopy (XPS) and ultraviolet photoelectron spectroscopy (UPS) were utilized for measurements. In **Figure 3**a, Zn 2p and S 2p peaks were observed from Alq_3/ZnS and Alq_3/ZnS/Cs_2CO_3 films in the XPS spectra, indicating that ZnS was deposited onto Alq_3. In addition, a Cs 3d peak was observed from Alq_3/ZnS/Cs_2CO_3 and Alq_3/Cs_2CO_3, indicating that ZnS and Cs_2CO_3 were properly deposited on the fabricated films. (The XPS spectra of each of the films are also included in Figure S1, Supporting Information.)

From the UPS spectrum, an increase in the binding energy of HOMO and a decrease in the vacuum level were observed in the Alq_3/ZnS/Cs_2CO_3 and Alq_3/Cs_2CO_3 films, differing from Alq_3 or Alq_3/ZnS films (Figure 3b,c). This result is similar to earlier results which demonstrated that the electron injection barrier decreases due to the charge transfer and n-type doping of the Alq_3 layer when Cs_2CO_3 is deposited on Alq_3 film.[25] However, the binding energy of HOMO and the vacuum level of Alq_3/ ZnS film without Cs_2CO_3 showed no significant

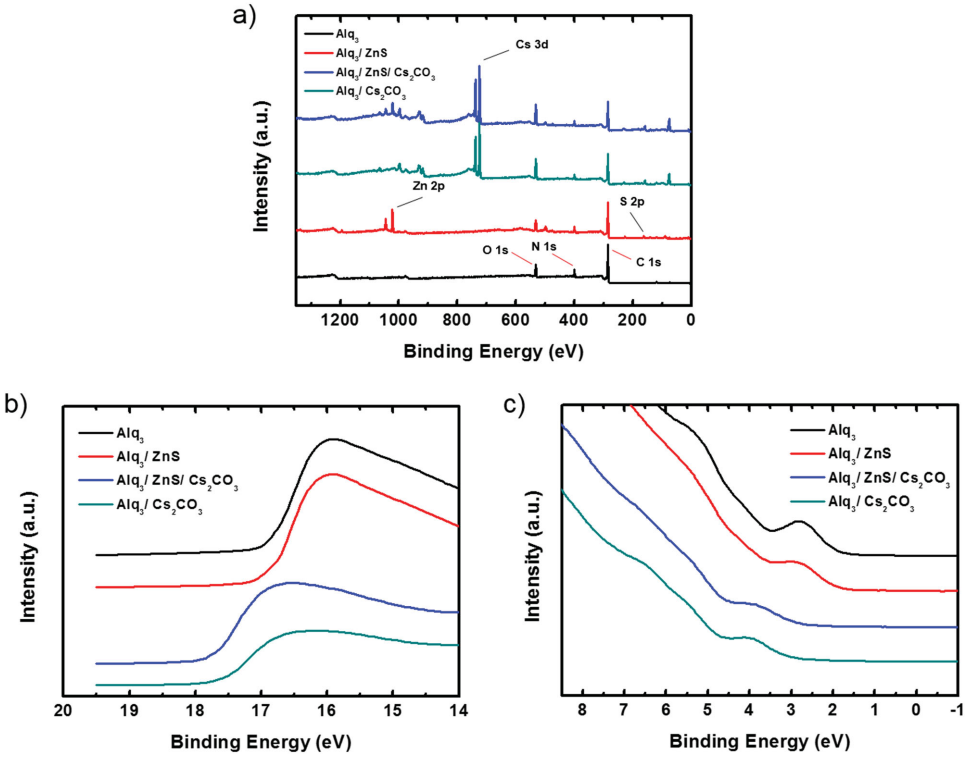

Figure 3. a) XPS spectra of Alq_3, Alq_3/ZnS, Alq_3/ZnS/Cs_2CO_3, and Alq_3/Cs_2CO_3 films. UPS spectra near b) the secondary electron cut-off and c) valance band of the Alq_3, Alq_3/ZnS, Alq_3/ZnS/Cs_2CO_3, and Alq_3/Cs_2CO_3 films.

changes compared to the film that contains only Alq_3. Furthermore, Alq_3/Cs_2CO_3, which is $Alq_3/ZnS/ Cs_2CO_3$ without ZnS, shows electronic properties similar to those of $Alq_3/ZnS/ Cs_2CO_3$. This shows that ZnS does not affect the electron injection property at the interface between Alq_3 and Cs_2CO_3. However, as the thickness of ZnS is increased, the electron injection ability is decreased, as shown in Figure 2b. Thus, it can be suggested that a carrier can tunnel through the barrier.

2.4. Flexibility of Multilayer Electrodes

The flexibility of the multilayer electrodes was investigated using a bending test under compressive strain. The stacked ZnS/Ag multilayer anode and $Alq_3/ZnS/Cs_2CO_3/Ag$ multilayer cathode were fabricated on 125 μm poly(ethylene terephthalate) (PET) substrate. Figure S2 of the Supporting Information shows the sheet resistance of the multilayer electrode and ITO electrode after 10 000 cycles bending at each bending radius. The bending radius was converted to strain considering the difference in electrode and substrate thickness.[29] The ITO electrode showed dramatically increased sheet resistance near the strain of 1% (around 120 Ω sq^{-1}). However, the sheet resistance of the multilayer electrodes after bending with strain over 1% was similar to that before bending (around 9 Ω sq^{-1}). This showed that the new multilayer electrodes are much more flexible than the ITO electrodes, and we could confirm that these multilayer electrodes could be used to achieve flexible OLEDs.

2.5. Improvement of Multilayer Electrode Using Optical Calculation

The multilayer electrodes improved the transmittance of OLEDs by using the antireflection. The dielectric layers, with high refractive indices and optimized thickness, cause antireflection by reducing the reflection on the surface of metal films. Therefore, in order to achieve this antireflection condition, the refractive indices and thickness of the ZnS layer (anode side, capping layer) are critical. The optical calculation was performed in relation to the thickness of the anode-side ZnS layer and the capping layer. The calculated optimal TFOLEDs structure is ZnS (y nm)/Ag (7 nm)/MoO_3 (5 nm)/NPB (50 nm)/Alq_3 (50 nm)/ZnS (3 nm)/Cs_2CO_3 (1 nm)/Ag (8 nm)/ZnS (x nm) on PET (125 μm) film. The calculation was conducted by transfer matrix using an E-field of multiple light reflections on each layer of the TFOLEDs. **Figure 4**a shows the calculated maximum transmittance of OLEDs was 75.2%, when

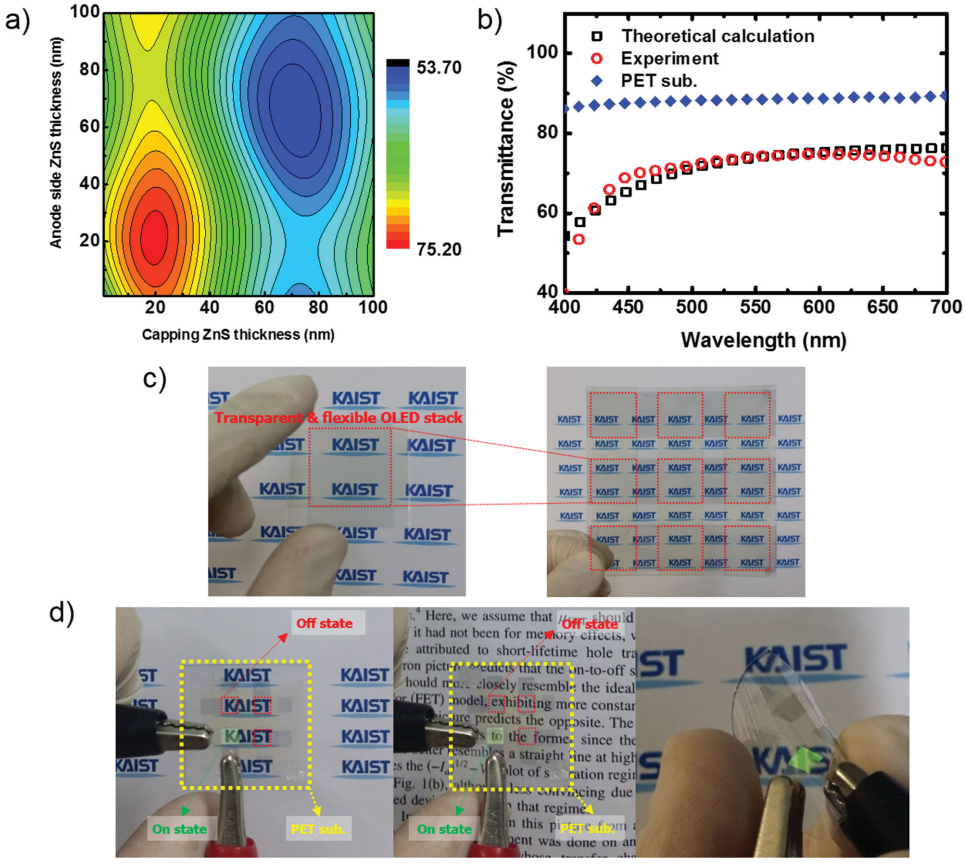

Figure 4. a) The calculated transmittance of TFOLEDs in relation to thicknesses of the ZnS layers (anode side and capping layer), b) Measured transmittance of the PET substrate and TFOLEDs, and calculated transmittance of the TFOLEDs (with anode ZnS 24 nm, capping layer ZnS 22 nm), c,d) Photographs of the fabricated TFOLEDs. c) TFOLED stack with 2.5 × 2.5 cm area and magnified images, d) photographs of TFOLEDs with on and off images with letters in the background (left and middle), and photograph of the TFOLEDs with bending (right).

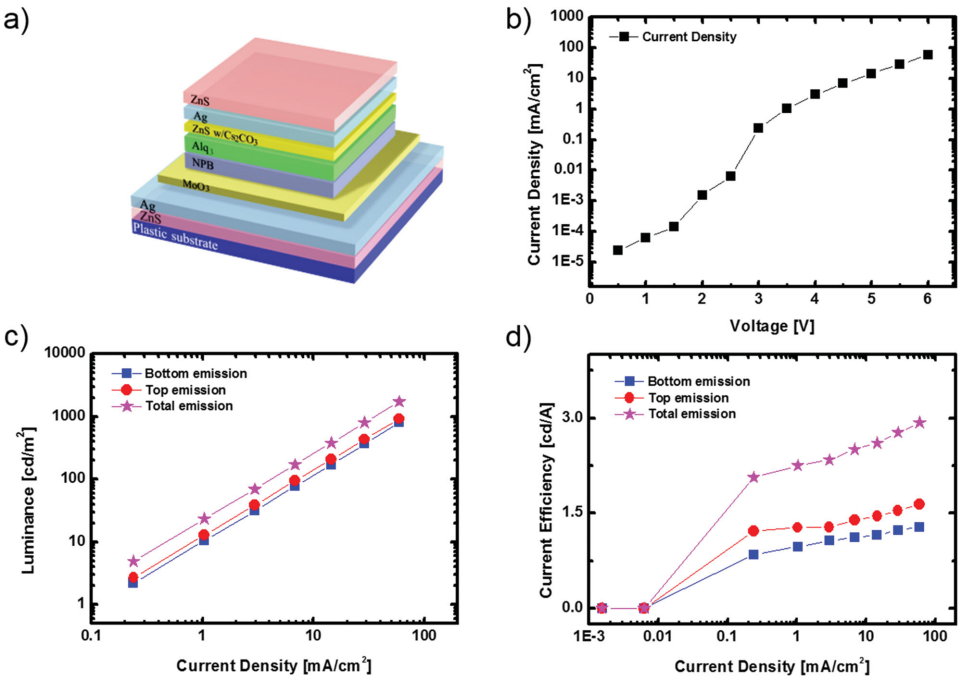

Figure 5. a) Schematic of the TFOLEDs, b) Current density–voltage (*J–V*) characteristics of the TFOLEDs, c) luminance–current density (*L–J*) characteristics and d) current efficiency–current density characteristics of the TFOLEDs. (Bottom emission is anode side; top emission is cathode side.)

the thickness of the anode side of the ZnS layer and the capping layer of ZnS, were 24 and 22 nm, respectively. In Figure 4b, the calculated transmittance of OLEDs with 24 nm ZnS anode side and a 22 nm capping layer shows quantitative agreement with the measured transmittance of TFOLEDs in the range of visible light. The peak transmittance was 74.22% around 550 nm and transmittance of over 70% was measured in the visible range. These results demonstrate the validity of the optical calculation, and that the fabricated TFOLEDs are highly transparent. This is remarkable considering that the device was fabricated on PET film (88% transparency to visible light) that is measurably less transparent than glass (92% in visible range).

In Figure 4c are images of the TFOLED stack (2.5 × 2.5 cm). The background letters can be seen clearly through TFOLEDs stack. Figure 4d shows the highly transparent, flexible newly fabricated OLEDs in the on and off states, and with bending.

2.6. Performance and Optical Properties of the TFOLEDs

From the experiments conducted to optimize the multilayer electrodes structure, we determined the optimal structure of the TFOLED to be (**Figure 5**a) ZnS (24 nm)/Ag (7 nm)/MoO_3 (5 nm)/NPB (50 nm)/Alq_3 (50 nm)/ZnS (3 nm)/Cs_2CO_3 (1 nm)/Ag (8 nm)/ZnS (22 nm), on PET (125 μm) film. Figure 5b shows the current density (*J*)–voltage (*V*) characteristics of the fabricated TFOLEDs. The turn-on voltage was 2.5 V and was not increased from that reported in previous work.[27] Moreover, conventional OLEDs have a light loss mechanism due to the difference in the refractive index values of the layers that comprise the OLEDs (the substrate mode and waveguide mode) and the surface plasmon mode. Particularly, a surface plasmon can arise at the interface between the metal and organic layers, and the surface plasmon loss is increased when Ag metal film is used for both the anode and the cathode. Therefore, considering the both-sides emission and surface plasmon loss, the efficiency of these TFOLEDs is higher than that of conventional OLEDs.[30] This means that fabrication of electron-only devices for modulating the thickness of Cs_2CO_3 and ZnS layers, and inserting the MoO_3 layer, was effective for maintaining the charge balance of the new TFOLEDs. The luminance and current efficiency of these TFOLEDs were measured including both bottom (substrate) and top (capping layer) emissions, as shown in Figure 5c,d. The total emission was the sum of bottom and top emission at the same current density. The values of luminance and current efficiency of bottom emission were slightly lower than that of the top emission, because of the emission loss from the PET on the bottom.

Figure 6a,b shows the external quantum efficiency (EQE) and power efficiency of the TFOLEDs. The values of EQE and power efficiency were similar to that of conventional OLEDs using NPB/Alq_3/LiF/Al. This might be from the effect of microcavities and not from the optimized structure of the TFOLEDs. OLEDs with strong microcavity effect show a significant blue shift of EL peaks with varying emission angle, due to the interference effect.[20,31] However, as shown in Figure 6c,d, the EL intensity spectra of bottom and top emissions at varying emission-angles show slight or no blue shift due to the high transparency of TFOLEDs. This indicates very little microcavity effect. In addition, the calculation of EL intensity for various thicknesses of Ag film was conducted to determine more precisely the microcavity effect (Figure S3, Supporting Information). The intensity value of the new TFOLEDs (7 nm anode, 8 nm cathode) lies between the calculated data for Ag-film thickness

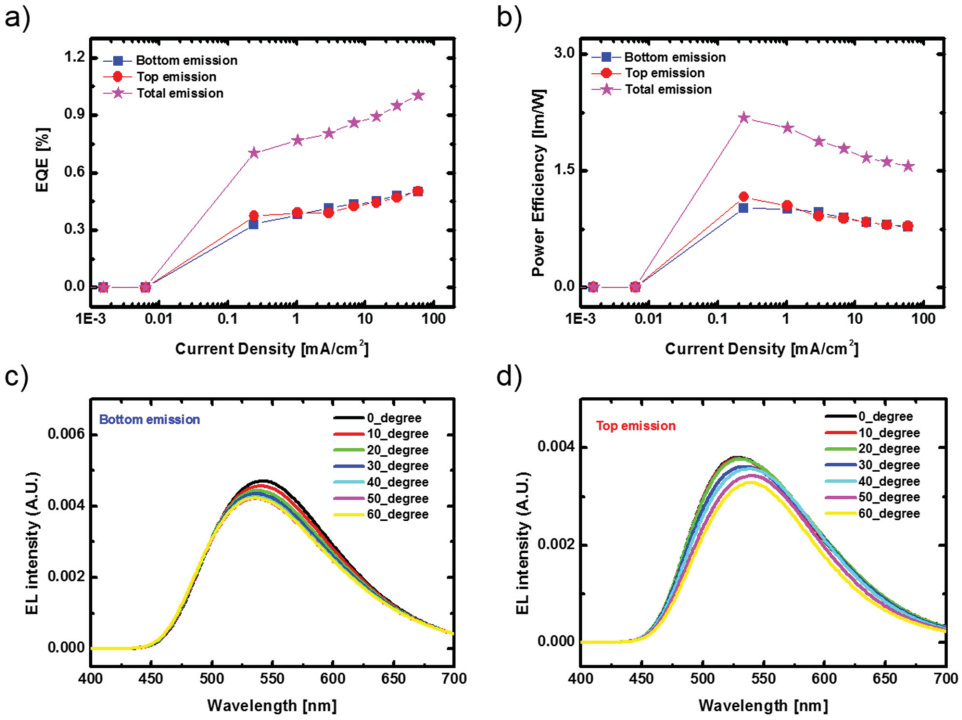

Figure 6. a,b) The EQE and power efficiency characteristics of the TFOLEDs: Bottom emission is anode side and top emission is cathode side. c,d) The EL spectra of the bottom emission and top emission of TFOLEDs with emission angles varying from 0° to 60° in increments of 10°.

of 5 and 10 nm, which shows that the measured intensity corresponds well with the calculations. Also, the TFOLEDs with relatively thick Ag film showed enhanced EL intensity due to the microcavity effect. These results show that the fabricated TFOLEDs exhibit only a weak microcavity effect, and that the optimized charge balance seems attributable to their high efficiency. In **Figure 7**a, the TFOLEDs show a nearly Lambertian emission pattern, and Figure 7b shows negligible change in the CIE coordinates at various angles. This means that the angular dependency problem from the microcavity effect can be solved in these TFOLEDs.

3. Conclusion

In summary, herein we propose highly transparent, flexible OLEDs incorporating multilayer electrodes. The fabricated TFOLEDs show improved transmittance and overcome the angular dependency caused by the microcavity effect. In order to improve the transmittance of TFOLEDs without efficiency degradation, the minimum film thickness for continuous Ag film was investigated by varying the number and kind of dielectric layers, and electron-only devices were fabricated to adjust the thickness of ZnS and Cs_2CO_3 layers for use in the

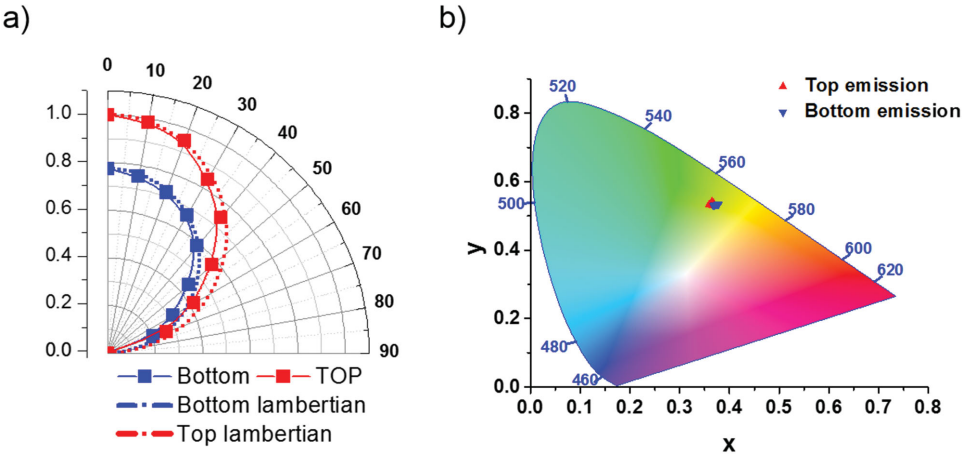

Figure 7. a) Radiant intensity profiles of TFOLEDs from bottom emission and top emission, b) change of CIE coordinates of bottom emission and top emission of TFOLEDs at different emission angles (0° to 60° with increments of 10°).

multilayer cathode. Moreover, optical calculations were performed to determine the optimal thicknesses of ZnS layers (anode side and capping layer) to promote antireflection. The optimized structures for TFOLEDs were fabricated on PET. The resulting device showed peak transmittance of 74.22% around 550 nm, and the measured transmittance was consistent with the calculated transmittance. The *J–V–L* characteristics of the proposed TFOLED design were similar to those reported in studies for which there was no degradation of efficiency. In addition, the TFOLEDs with flexible multilayer electrodes were flexible under compressive stress. The EL intensity spectra and CIE coordination at varying emission angles showed negligible shift, and calculations of the influence of the microcavity effect was also negligible because of the high transmittance of these devices. Therefore, we consider the proposed TFOLED design a promising candidate (overcoming limitations found in previous work) for use in transparent, flexible displays.

4. Experimental Section

Fabrication of TFOLEDs with Multilayer Anode and Cathode: Multilayer anodes with ZnS (20 nm), Ag (× nm) layers were deposited using a thermal evaporation system with a 2 Å s^{-1} deposition rate. The sheet resistance was measured by 4-probe and the surface morphology of the multilayer anode was examined using SEM (PEI Company, Magellan400). The surface energy of the dielectric layers was determined using the Owen–Wendt method by measuring the contact angles of liquid drops (H_2O, CH_2I_2) resting on the surfaces of the dielectric layers. The contact angles were measured using a contact angle analyzer from SEO Co., Ltd. (Phoenix300 plus). The XPS and UPS spectra were measured using multipurpose X-ray photoelectron spectroscopy with UPS (Thermo VG Scientific). The UPS spectra were obtained using He I (21.2 eV) as an excitation source, and the samples were biased at –10 V to observe the vacuum level. The XPS spectra were measured using Al *Kα* (1486.6 eV) as the radiation source. The structure of the multilayer cathode was determined by the *J–V* characteristics of electron-only devices. The structure of electron-only devices was Al (100 nm), Alq_3 (50 nm), ZnS (*x* nm), Cs_2CO_3 (*x* nm), and Ag (100 nm), with split Cs_2CO_3 and ZnS layers. The *J–V* characteristics were measured using a Keithley 2400 source meter. The sheet resistance and surface morphology of the multilayer cathode were measured in the same way for the multilayer anode.

Flexibility and Transmittance of the Multilayer Electrode: The ZnS (20 nm) and Ag (7 nm) layers of the multilayer anode, and Alq_3 (30 nm), ZnS (3 nm), Cs_2CO_3 (1 nm), and Ag (8 nm) layers of the multilayer cathode were deposited on PET (125 μm) for measurement of flexibility. The flexibility of the multilayer electrode and ITO film was compared using a bending test (bending machine by Labtech Science Co., Ltd.) under compressive stress with bending radius of 5, 10, 15, or 20 mm. After 10 000 repetitions, the enhancement of the sheet resistance of the multilayer and ITO films was measured using a 4-probe.

Before fabricating the highly transparent, flexible OLEDs, optical calculations were done to improve the transmittance using the MATLAB simulation tool (MathWorks, Inc.). From the simulation tools, the electric field was calculated by transfer matrix. The thickness of the dielectric layers (ZnS layer, Ag anode side; ZnS capping layer) were calculated with which each device showed the highest transmittance. The transmittance spectra of the TFOLEDs (range of visible light) were obtained using an UV–vis spectrophotometer (UV-2550, Shimadzu). The baseline was estimated in comparison to transmittance through air.

Fabrication and Characterization of TFOLEDs: The highly transparent and flexible OLEDs were fabricated on PET (125 μm) substrate. The layer-structure of the TFOLED devices was ZnS (24 nm), Ag (7 nm), MoO_3 (5 nm), NPB (50 nm), Alq_3 (50 nm), ZnS (3 nm), Cs_2CO_3 (1 nm), Ag (8 nm), and ZnS (22 nm). All the layers were deposited by thermal evaporation. Characteristics of the TFOLEDs (i.e., *J–V–L* curve, emission spectra, EQE, and power efficiency) were measured using a Keithley 2400 source meter and a spectroradiometer (CS-2000, Konica Minolta) together. In addition, in order to obtain EQE and power efficiency, angular emission spectra were measured from –60° to 60° with increments of 10°.

Supporting Information

Supporting Information is available from the Wiley Online Library or from the author.

Acknowledgements

D.-Y.K. and Y.C.H. contributed equally to this work. This work was supported by the National Research Foundation of Korea (NRF) grant funded by the Korea government (MSIP) (CAFDC 5–1(0), NRF-2007–0056090) and project (R&BD for the large area transparent flexible electrode film and production process) from Korea Advanced Institute of Science and Technology (KAIST) grant funded by Korea government (MSIP) (N01150032). The authors also would like to acknowledge support from LG Display Co., Ltd.

Received: June 22, 2015
Revised: July 21, 2015
Published online: November 2, 2015

[1] a) J. F. Wager, *Science* **2003**, *300*, 1245; b) G. Gustafsson, Y. Cao, G. M. Treacy, F. Klavetter, N. Colaneri, A. J. Heeger, *Nature* **1992**, *357*, 477.
[2] G. Gu, Z. L. Shen, P. E. Burrows, S. R. Forrest, *Adv. Mater.* **1997**, *9*, 725.
[3] D. R. Cairns, R. P. Witte, D. K. Sparacin, S. M. Sachsman, D. C. Paine, G. P. Crawford, R. R. Newton, *Appl. Phys. Lett.* **2000**, *76*, 1425.
[4] Y. Zhu, J. M. Tour, *Nat. Photonics* **2012**, *6*, 72.
[5] J. Meyer, P. Gorrn, S. Hamwi, H. H. Johannes, T. Riedl, W. Kowalsky, *Appl. Phys. Lett.* **2008**, *93*, 073308.
[6] a) X. Y. Zeng, Q. K. Zhang, R. M. Yu, C. Z. Lu, *Adv. Mater.* **2010**, *22*, 4484; b) J. Y. Lee, S. T. Connor, Y. Cui, P. Peumans, *Nano Lett.* **2008**, *8*, 689.
[7] a) M. G. Kang, L. J. Guo, *Adv. Mater.* **2007**, *19*, 1391; b) S. M. Lee, J. S. Chae, D. Y. Kim, K. C. Choi, *Org. Electron.* **2014**, *15*, 3354.
[8] a) S. Bae, H. Kim, Y. Lee, X. F. Xu, J. S. Park, Y. Zheng, J. Balakrishnan, T. Lei, H. R. Kim, Y. I. Song, Y. J. Kim, K. S. Kim, B. Ozyilmaz, J. H. Ahn, B. H. Hong, S. Iijima, *Nat. Nanotechnol.* **2010**, *5*, 574; b) J. B. Wu, M. Agrawal, H. A. Becerril, Z. N. Bao, Z. F. Liu, Y. S. Chen, P. Peumans, *ACS Nano* **2010**, *4*, 43; c) K. S. Kim, Y. Zhao, H. Jang, S. Y. Lee, J. M. Kim, K. S. Kim, J. H. Ahn, P. Kim, J. Y. Choi, B. H. Hong, *Nature* **2009**, *457*, 706; d) F. Bonaccorso, Z. Sun, T. Hasan, A. C. Ferrari, *Nat. Photonics* **2010**, *4*, 611.
[9] a) Z. C. Wu, Z. H. Chen, X. Du, J. M. Logan, J. Sippel, M. Nikolou, K. Kamaras, J. R. Reynolds, D. B. Tanner, A. F. Hebard, A. G. Rinzler, *Science* **2004**, *305*, 1273; b) M. W. Rowell, M. A. Topinka, M. D. McGehee, H. J. Prall, G. Dennler, N. S. Sariciftci, L. B. Hu, G. Gruner, *Appl. Phys. Lett.* **2006**, *88*, 233506.
[10] a) S. A. Carter, M. Angelopoulos, S. Karg, P. J. Brock, J. C. Scott, *Appl. Phys. Lett.* **1997**, *70*, 2067; b) W. H. Kim, A. J. Makinen, N. Nikolov, R. Shashidhar, H. Kim, Z. H. Kafafi, *Appl. Phys. Lett.* **2002**, *80*, 3844.

[11] T. Eisenhammer, M. Lazarov, M. Leutbecher, U. Schoffel, R. Sizmann, *Appl. Opt.* **1993**, *32*, 6310.
[12] J. C. C. Fan, F. J. Bachner, *Appl. Opt.* **1976**, *15*, 1012.
[13] X. J. Liu, X. Cai, J. S. Qiao, H. F. Mao, N. Jiang, *Thin Solid Films* **2003**, *441*, 200.
[14] M. Zadsar, H. R. Fallah, M. H. Mahmoodzadeh, S. V. Tabatabaei, *J. Lumin.* **2012**, *132*, 992.
[15] H. Kermani, H. R. Fallah, M. Hajimahmoodzadeh, *Physica E* **2013**, *47*, 303.
[16] H. Cho, J. M. Choi, S. Yoo, *Opt. Express* **2011**, *19*, 1113.
[17] D. Y. Yang, S. M. Lee, W. J. Jang, K. C. Choi, *Org. Electron.* **2014**, *15*, 2468.
[18] a) T. Winkler, H. Schmidt, H. Flugge, F. Nikolayzik, I. Baumann, S. Schmale, T. Weimann, P. Hinze, H. H. Johannes, T. Rabe, S. Hamwi, T. Riedl, W. Kowalsky, *Org. Electron.* **2011**, *12*, 1612; b) T. Winkler, H. Schmidt, H. Flugge, F. Nikolayzik, I. Baumann, S. Schmale, H. H. Johannes, T. Rabe, S. Hamwi, T. Riedl, W. Kowalsky, *Thin Solid Films* **2012**, *520*, 4669; c) Y. C. Han, M. S. Lim, J. H. Park, K. C. Choi, *IEEE Electron Device Lett.* **2014**, *35*, 238.
[19] a) D. Poitras, C. C. Kuo, C. Py, *Opt. Express* **2008**, *16*, 8003; b) H. J. Peng, J. X. Sun, X. L. Zhu, X. M. Yu, M. Wong, H. S. Kwok, *Appl. Phys. Lett.* **2006**, *88*, 073517.
[20] C. H. Cheung, A. B. Djurisic, C. Y. Kwong, H. L. Tam, K. W. Cheah, Z. T. Liu, W. K. Chan, P. C. Chui, J. Chan, A. D. Rakic, *Opt. Commun.* **2005**, *248*, 287.
[21] N. P. Sergeant, A. Hadipour, B. Niesen, D. Cheyns, P. Heremans, P. Peumans, B. P. Rand, *Adv. Mater.* **2012**, *24*, 728.
[22] Y. C. Han, M. S. Lim, J. H. Park, K. C. Choi, *Org. Electron.* **2013**, *14*, 3437.
[23] N. Formica, D. S. Ghosh, A. Carrilero, T. L. Chen, R. E. Simpson, V. Pruneri, *ACS Appl. Mater. Interfaces* **2013**, *5*, 3048.
[24] M. T. Lee, C. H. Liao, C. H. Tsai, C. H. Chen, *Adv. Mater.* **2005**, *17*, 2493.
[25] a) M. H. Chen, C. I. Wu, *J. Appl. Phys.* **2008**, *104*, 113713; b) J. S. Huang, Z. Xu, Y. Yang, *Adv. Funct. Mater.* **2007**, *17*, 1966.
[26] a) W. Y. Wong, G. J. Zhou, X. M. Yu, H. S. Kwok, B. Z. Tang, *Adv. Funct. Mater.* **2006**, *16*, 838; b) H. M. Zhu, T. Q. Lian, *Energy Environ. Sci.* **2012**, *5*, 9406.
[27] a) C. S. Choi, S. M. Lee, M. S. Lim, K. C. Choi, D. Kim, D. Y. Jeon, Y. Yang, O. O. Park, *Opt. Express* **2012**, *20*, A309; b) J. Y. Kim, C. S. Choi, W. H. Kim, D. Y. Kim, D. H. Kim, K. C. Choi, *Opt. Express* **2013**, *21*, 5424.
[28] a) J. Kim, M. Kim, J. W. Kim, Y. Yi, H. Kang, *J. Appl. Phys.* **2010**, *108*, 103703; b) Y. S. Zhao, C. A. Di, W. S. Yang, G. Yu, Y. Q. Liu, J. N. Yao, *Adv. Funct. Mater.* **2006**, *16*, 1985.
[29] Z. Suo, E. Y. Ma, H. Gleskova, S. Wagner, *Appl. Phys. Lett.* **1999**, *74*, 1177.
[30] a) C. S. Choi, D. Y. Kim, S. M. Lee, M. S. Lim, K. C. Choi, H. Cho, T. W. Koh, S. Yoo, *Adv. Opt. Mater.* **2013**, *1*, 687; b) D. Y. Kim, C. S. Choi, J. Y. Kim, D. H. Kim, K. C. Choi, *Org. Electron.* **2014**, *15*, 1222.
[31] a) A. Dodabalapur, L. J. Rothberg, R. H. Jordan, T. M. Miller, R. E. Slusher, J. M. Phillips, *J. Appl. Phys.* **1996**, *80*, 6954; b) S. Dirr, S. Wiese, H. H. Johannes, D. Ammermann, A. Bohler, W. Grahn, W. Kowalsky, *Synth. Met.* **1997**, *91*, 53; c) R. H. Jordan, L. J. Rothberg, A. Dodabalapur, R. E. Slusher, *Appl. Phys. Lett.* **1996**, *69*, 1997.